Proceedings of the 2008 IEEE
International Workshop on Safety, Security and Rescue Robotics
Sendai, Japan, October 2008

Hyperspectral Imaging for Victim Detection with Rescue Robots

Marina Trierscheid, Johannes Pellenz, Dietrich Paulus
University of Koblenz-Landau
Universitätsstr. 1
56070 Koblenz, Germany
{mtrierscheid, pellenz, paulus}@uni-koblenz.de

Dirk Balthasar
TiTech GmbH
Otto-Hahn-Straße 6
56218 Mülheim-Kärlich, Germany
balthasar@titech.com

Abstract — The main task of rescue robots is to locate victims after a desaster such as an earthquake. For this task sensor data is used to localize the robots in their environment, build maps, and mark the victims in the maps. Usually, thermal and color cameras, monitored by a human operator, are used for the detection.

Hyperspectral imaging techniques are today used for industrial tasks such as quality control, fast material sorting or food analysis. This paper proposes a new approach for the victim detection in rescue environments, based on hyperspectral imaging in the near infrared spectral domain. This technique involves a simultaneous recording of spatial and spectral information. Different materials can be distinguished when the spectra are analyzed.

The result of the experiments show that the spectra of skin are very characteristic and that even under the impact of ash layers the spectral similarity remains very high. Thus our approach can be used for rescue robots to find human bodies autonomously, where other techniques such as color or thermal image analysis would fail.

Keywords: *Robotics, Rescue Robotics, RoboCup Rescue, USAR, spectral imaging, hyperspectral imaging, spectral analysis, NIR, body detection*

I. Introduction

In emergency cases, such as after the collapse of the World Trade Center in 2001, rescue robots have to fulfill several complex tasks. They have to explore an environment that is highly destructed and find victims; some robots also build a map including obstacles. The detection of victims is the most important task for rescue robots and this feature makes them most attractive [7, p. 1152, 1160].

Most of the techniques for victim detection today are based on color vision, e. g. the detection of skin color, faces, or movement. Other common approaches are the detection of body heat, voices, and breathing (CO_2 detection).

Spectral imaging in the sense of analyzing radiation other than the visible light has by now primarily been used for heat detection. Body heat is in the wavelength of infrared (IR) so that infrared sensors can be used to identify it. This technique is very robust but cannot be used solitarily because other heat sources would likely also be detected. In a sufficiently warm environment (around $37°C$) heat as a sign of a human body would even fail completely.

Vision based techniques for victim detection strongly depend on the illumination, especially when color is analyzed.

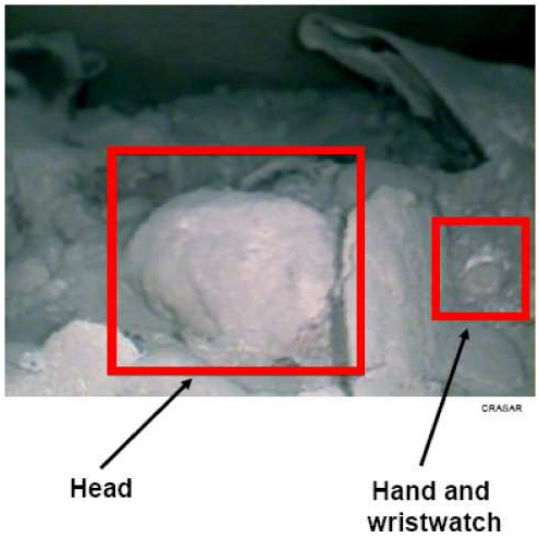

Fig. 1. Victim in the World Trade Center after the collapse 2001 [11], courtesy of Dr. Robin R. Murphy

When it comes to fog or dust covering (which is a very common factor in real catastrophe scenarios) vision based approaches will also fail. Fig. 1 shows an image captured by a rescue robot in the World Trade Center in 2001 after 9/11. ”Even experienced human rescuers failed to identify the victim in the real-time video stream from a rescue robot” [11].

Hyperspectral IR imaging produces images that contain a contiguous spectrum in the bandwidth of IR on a spatial scanline in the scene. This is a relatively new development and has its background in optical spectroscopy. Hyperspectral imaging for the first time provides the technique to combine spectroscopy and image processing. Today this technique is used in chemical analysis for the identification and quantification of a sample’s constitution [3, p. 9]. Other fields of application are food analysis, quality control, observation in the production industry and fast material sorting, e. g. in the recycling industry, where the hyperspectral cameras are geared towards an assembly line [2], [6].

One benefit of hyperspectral imaging with respect to thermal images for victim detection is that it is independent

978-1-4244-2032-2/08/$25.00 ©2008 IEEE.

of temperature. Thus, also cold bodies (dead persons) can be detected. Using the bandwidth of near infrared (NIR), where the radiation has shorter wavelengths, has the additional advantage that it has a high depth of penetration into the sample, which can be useful to solve the problem of dust coverings in rescue environments [4, p. 5].

In our work we focused on the preprocessing of hyperspectral NIR images and the classification of human bodies. The preprocessing step is important, because defect pixels in the images and dark current affect the signal. The corrected spectra of known objects are then used to train a classifier for different materials. Finally, in the classification step materials such as skin, hair, or clothes can be detected and distinguished from other materials in home or office environments such as wood or plastics.

II. State of the art

A. Hyperspectral Imaging

1) Fundamentals: Hyperspectral imaging combines the rich information available from spectroscopy with the ability to acquire this information in a spatially resolved manner. The most common variant of hyperspectral imaging captures the bandwidth of IR radiation. This technique has its seeds in optical spectroscopy, a field of chemistry, where the interaction between electromagnetic waves and both living and dead matter is analyzed [10].

In optical IR spectroscopy a sample is irradiated with electromagnetic waves in the bandwidth of IR. During the irradiation the molecules of the sample absorb light quanta in particular bandwidths, depending on the molecular structure of the substance. This causes the molecules to start swinging or rotating. An optical spectrometer points towards the substance and measures the diffusely reflected light in the wavelength of the IR. The result of the measurement is a spectrum which displays the intensity of the transmitted light (transmission spectrum) respectively the distribution of the reflected light (absorption spectrum) in the considered wavelength range. Thus most substances show a characteristic spectrum in the IR [10]. In the absorption spectra the positions of absorption bands – bandwidths, where much radiation has been absorbed – are characteristic for the kind of material.

With the availability of 2D NIR detectors, it is now possible to measure not only a spectrum at one position but whole scanlines of spectra with more than one hundred channels, where one channel corresponds to the response radiation of one wavelength.

2) Infrared Radiation: Infrared radiation is electromagnetic radiation with longer wavelengths than the visible light and shorter wavelengths than tetrahertz radiation and microwaves. Fig. 2 shows the common subdivision of the IR radiation, which results from different properties and detection technologies of the wavelength ranges.

NIR radiation - which we analyze in our approach - has shorter wavelengths than the MIR and FIR radiation, which is why it is more energetic and thus has a stronger penetration depth. That means that not only the radiation reflected from the surface of the sample but also the layers beneath, up to some mm, constitute the NIR-spectra. This property makes the technique applicable for the victim detection in dust or ash covered environments. Another property of NIR radiation is that many chemical functional groups show a specific oscillation under the influence of NIR radiation. These oscillations can be assigned to absorption bands in defined bandwidths of the NIR spectrum, which is why substances consisting of these functional groups can be identified easily [5, p. 30]. Some of these substances are organic molecules such as fats, carbohydrate and proteins. Another group includes synthetic materials such as PVC or PET.

Name	**Abbreviation**	**Wavelength** $[\mu m]$
Near Infrared	NIR	0.78 - 3
Middle Infrared	MIR	3 - 50
Far Infrared	FIR	50 - 1000 (= 1mm)

Fig. 2. Subdivision of the infrared radiation (DIN 5031)

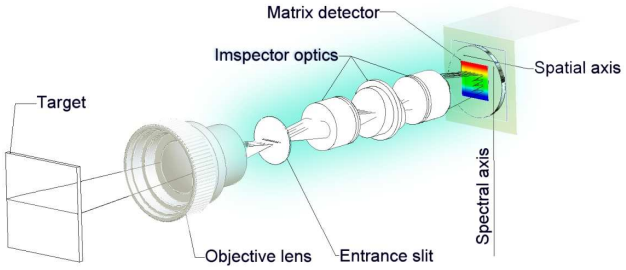

Fig. 3. Principle of the line scan camera ImSpector N17E, courtesy of Specim.

B. Hyperspectral NIR Camera ImSpector

The camera used in our experiments is a hyperspectral NIR line scan camera (Specim[1] ImSpector N17E). The principle of the camera can be seen in Fig. 3. In contrast to a common optical camera it only captures one scanline of the scene at a time. Inside the camera the light that passes the objective lens and the entrance slit of the spectrograph is dispersed into its NIR spectrum. The spectrograph is based on a prism-grating-prism (PGP) component. The FPA (Focal Plane Array) camera connected to the spectrograph captures and digitizes the NIR spectrum with 60 Hz. The sensors on the FPA are InGaAs (Indium Gallium Arsenid) photodiodes that are sensitive in the NIR. In order to preserve a stable temperature the sensor is cooled consistently. The detected wavelength bandwidth of the ImSpector is 0.9 μm to 1.7 μm. The resulting image has a size of 320 $\times$ 256 pixels and has its spatial resolution on the x axis and its spectral resolution on the y axis. Thus each column in the image corresponds to one NIR spectrum, which is depicted in Fig. 4. The camera has a size of 350 $\times$ 100 $\times$ 130 mm and a weight of 4.5 kg.

[1] http://www.specim.fi

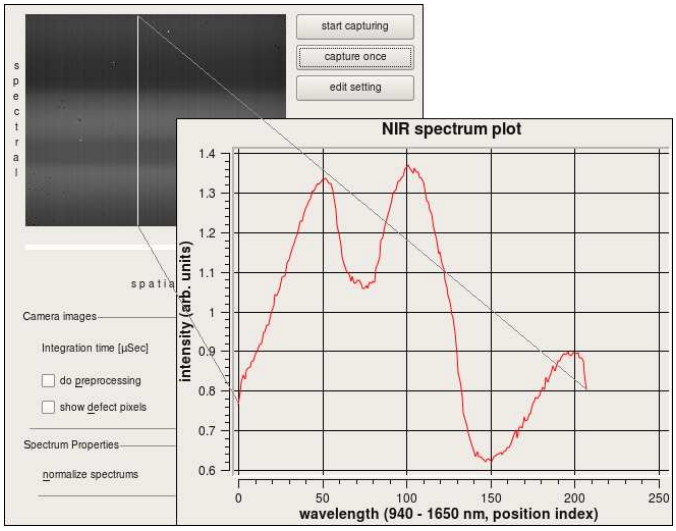

Fig. 4. A hyperspectral image and the plot of one spectrum.

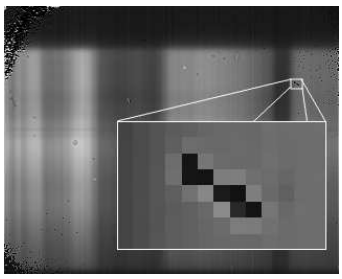

Fig. 5. Defect pixels in a hyperspectral image.

Besides the adjustment of the objective the integration time of the capturing process can be continuously regulated by the software. The integration time corresponds to the exposure time of photographic cameras.

C. Defect Pixel Interpolation

The images obtained from the hyperspectral camera need to be preprocessed properly to get comparable datasets and to achieve a stable classification. Fig. 5 shows that the camera images have many defects, which result from bad bondings from the light sensitive material to the electronics, and dark borders at the top and at the bottom. The dark borders are caused by displacements resulting from the integration of the spectrograph and the FPA camera, so these areas do not contain any relevant information and can be ignored. However, the single defect pixels can be corrected by an algorithm that uses the Fourier transform of an image and was first applied in medical image processing for the correction of flat panel images in [1].

The algorithm requires the locations of the defect pixels to be known. Then it runs iteratively over the image, does a lowpass filtering in the frequency domain and replaces the defect pixels in the original image by the pixels of the lowpass filtered image. Thus in each iteration the following steps are executed:

1) Transform the original image from the spatial to the frequency domain via the two-dimensional discrete Fourier transform.
2) Delete the high frequencies in the transformed image (using a constant threshold).
3) Transform the frequence image back to the spatial domain.
4) Copy the pixels at the defect-pixels-locations from the back-transformed image into the original image.
5) Repeat from step 1 until the changes made in the original image are smaller than a threshold.

Using the Fourier transform for the reconstruction gives much better results than a linear interpolation because the image represented as its amplitudes and frequencies offers the possibility to reconstruct the image signal using similar parts of the image signal itself. Thus the signal is reconstructed adaptively.

D. Non-Uniformity and Dark Current Compensation

Infrared FPA detectors are known to produce a non-uniform response, which leads to images with a fixed bias pattern. Furthermore the image is influenced by dark current; it is the result of a constant response of the detectors when they are not exposed to light. The simplest method to compensate for the dark current is to capture a dark image, with the lens of the camera covered, and later substract the pixel values of the dark reference from the corresponding pixel value in each image. In order to get the rate of the maximum intensity of each pixel in the camera images a white reference image is captured. Then each value in the captured images is divided by the corresponding value in the white reference. In order to capture this reference one illuminates a white reference material such as a barium sulfate tile and captures an image only showing the tile. Barium sulfate has the property that with over 90% it has a very high reflectivity in the radiation bandwith of about 0.25 to 2.5 μm, which includes the bandwith of NIR [12]. The combination of these two steps results in the actual reflectance image of a sample [6]:

$$\forall p_{ij} \in I : \ \hat{p}_{ij} = \frac{p_{ij} - d_{ij}}{w_{ij} - d_{ij}} \tag{1}$$

Here p_{ij} is the pixel value at position (i, j) in the sample image I, $\hat{p}_{ij}$ a pixel value in the output image $\hat{I}$, d_{ij} a pixel value in the dark reference image and w_{ij} a pixel value in the white reference image.

E. Noise Reduction

Noise reduction is another important aspect of the hyperspectral image preprocessing because noise distorts the image signal and affects the further processing.

Classical noise reduction techniques involve smoothing filters such as the linear moving average or Gauss filter or the non linear median filter (moving averages). They are especially effective for time domain encoded signals. Applied to spectra these filters have the disadvantage that not only the noise is reduced but also peaks of the signal are diminished. However

high or low moments are often a characteristic feature of the spectrum and should be retained [8].

A common approach for data smoothing of spectral data is provided by the Savitzky-Golay filter which is based on the least squares polynomial fitting across a moving window [9]. The idea is not to approximate the data in the moving window by a constant – which results in averaging – but by a polynomial of higher order: Let $\boldsymbol{A}$ be the design matrix for the problem of fitting a polynomial of degree M in i to the data values $f_{-n_\mathrm{L}}, \ldots, f_{n_\mathrm{R}}$, where n_L is the number of considered previous data points and n_R the number of considered subsequent data points.

$$A_{ij} = i^j \quad with\ i = -n_\mathrm{L}, \ldots, n_\mathrm{R}, \quad j = 0, \ldots, M \tag{2}$$

Based on this matrix the following equation is used to calculate the Savitzky-Golay filter coefficients:

$$c_n = \sum_{m=0}^{M} \left\{ (\boldsymbol{A}^\mathrm{T} \cdot \boldsymbol{A})^{-1} \right\}_{0m} n^m \tag{3}$$

The index of the inverse matrix indicates that only one row is used for the computation. The data vector to be approximated is replaced by the unit vector so the coefficients can be calculated once in advance and then be applied to the real data by using them as the coefficients of a simple linear electronic filter. The algorithm can be found in [8].

F. Classification Algorithms

There are a lot of techniques which can be used to classify hyperspectral data sets. A simple example for such a classifier would be the calculation of sum-squared differences (SSD) of normalized spectra; a more sophisticated one would be a support vector machine (SVM). [6] evaluated some other classification algorithms suitable for NIR hyperspectral images: the Linear and Quadratic Discriminant Classifier (LDC, QDC), the Fisher Linear Discriminant Classifier (FLDC) and the Spectral Angle Mapper (SAM). Their domain of application was polymer sorting. The result of the evaluation was that the SAM is the preferable method for this application.

The SAM is a simple mapper algorithm which does not involve statistical evaluation. Instead, the reference and the sample spectrum are treated as vectors in the n-dimensional space and the angle between the two vectors is taken to constitute the spectral similarity. Equation (4) shows how the multi-dimensional angle can be computed [13]:

$$\varphi = \arccos \left(\frac{\sum_{i=1}^{n} t_i r_i}{\sqrt{\sum_{i=1}^{n} t_i^2} \cdot \sqrt{\sum_{i=1}^{n} r_i^2}} \right) \tag{4}$$

where n is the number of bands in the spectrum, t_i is the test spectrum, and r_i the reference spectrum.

III. Implementation

We developed an application that controls the ImSpector camera described in Sect. II-B. In addition, it preprocesses the hyperspectral images and classifies the spectra using the techniques presented in Sect. II.

A. Setup and Reference Images

The ImSpector camera has been connected to a PC via USB. For our experiments we use a standard 500 W halogen headlight for irradiation so that a high rate of radiation is reflected by the sample and captured by the camera. However, on our mobile system, we will install an adjusted light source, which focuses on the area that is seen by the camera.

The reference images have been captured as described in Sect. II-D. We chose the integration time for both images in a way that the resulting image was as bright as possible but without having blooming effects which result from too high intensities. An integration time of 25000 μs in combination with a uniform illumination delivered good results.

B. Hyperspectral Image Preprocessing

Since the specific camera we used has many defect pixels, particularly at the borders, and dark borders at the top and the bottom (see Fig. 5), we only considered a sub-image of the original image for the further processing. Thus we reduced the image size from 320 $\times$ 256 to 256 $\times$ 208 pixels.

1) Defect Pixel Localization: In order to correct the remaining defect pixels their location must first be detected. This localization was done using the white and dark reference and two sample images. For both reference images we chose an appropriate threshold to find the locations of constant white and dark pixels. Further elements whose pixel values remain constant were detected by subtracting two sample images captured with different integration times and using a threshold on the subtraction image. Pixels below the threshold are considered to be defect.

Since the defect pixel elements slightly affect their neighbors (as can be seen in Fig. 5), the location of their 4 neighbors were marked defect, too.

2) Defect Pixel Interpolation: Since the location of the defect pixels could be computed in advance we implemented the adaptive frequency based correction algorithm presented in Sect. II-C, using the Fast Fourier Transform (FFT) algorithm for the transformation into the frequency domain. Note that both dimensions of the image are used for the reconstruction, so here, both the spectral and spatial information is used.

3) Non-Uniformity and Dark Current Compensation: After the defect pixel correction of the white and dark reference image and the current sample image we calculated the actual rate of reflectance according to Sect. II-D. We call the result the ”normalized image”.

4) Noise Reduction: We implemented the Savitzky-Golay filter as described in Sect. II-E and applied it to the normalized image, but only along the spectral dimension. We used the order of polynomial n = 4 and a mask size of 9 pixels. The

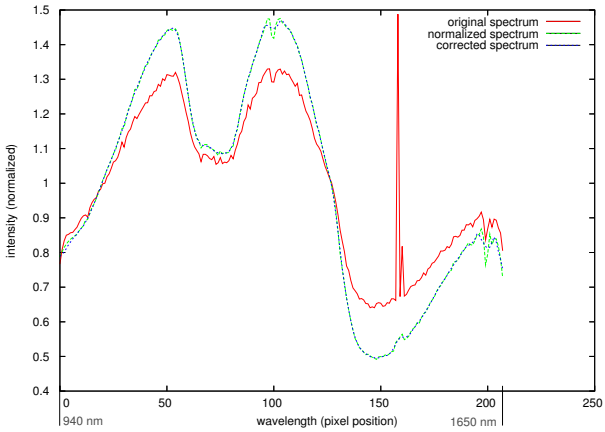

Fig. 6. Spectrum plot. First curve: spectrum in original image; second curve: spectrum after defect pixel correction and normalization; third curve: spectrum after all preprocessing steps.

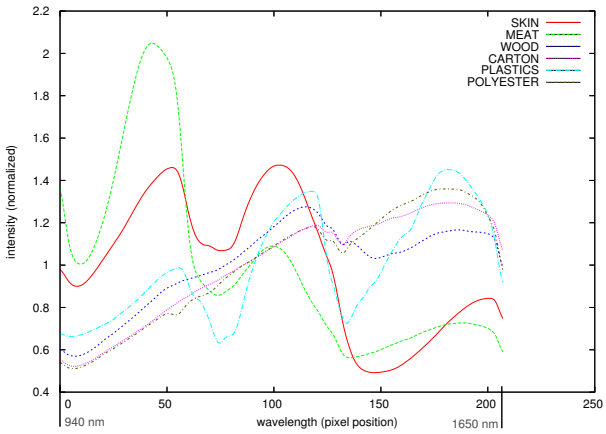

Fig. 7. The reference spectra used to calculate the spectral angle of a sample spectrum.

following table shows the corresponding filter coefficients (the second half is omitted because of symmetry).

n	Savitzky-Golay coefficients				
4	0.035	-0.128	0.070	0.315	0.417

The result of all the preprocessing steps can be seen exemplarily at one spectrum in Fig. 6.

C. Classification

In order to get an idea, how discriminative the NIR spectra of different materials are, we implemented a simple classifier. Following the evaluation of [6] (see Sect. II-F), we implemented the SAM (Spectral Angle Mapper) algorithm. Our training set is composed of hyperspectral images from different materials, such as skin, clothes, and wood. It is important that each image only shows one kind of material because in the training step we average the spectral data. At the start of the application the images are loaded into the trainer, stating their particular class. After the image preprocessing every single spectrum is scaled by its mean value norm to eleminate intensities. Then the spectral data are averaged along the spatial domain in order to obtain one reference spectrum per class. For each material several images can be trained, which leads to a more stable classification. In the classification step the sample image is preprocessed, then each spectrum of the image is tested against each reference spectrum of the classifier by computing the spectral angle. The smallest angle in combination with a threshold constitutes the resulting material of the particular spectrum in the image. Thus several materials can be detected in a single hyperspectral image.

IV. Results

We trained our SAM classifier with 2 to 3 different hyperspectral images of each class (one image contains 256 spectra). As sample materials for victim detection we chose human skin, meat (pork tartare), and polyester cloth. Other materials such as plastics, wood, and carton were chosen as samples for the environment in buildings. The reference spectrum of each material is shown in Fig. 7. The following table shows the classification results. The rows correspond to the analyzed samples and the columns to the material classes. The percent values are related to the rate of spectra of the samples which have been classified as the particular material. We applied a threshold of $15°$ to the result of the SAM, so that spectrums with a greater spectral angle were classified as ”unknown”.

	material classes						
samples	skin	meat	polyester	plastics	wood	carton	unknown
arm	100%	0%	0%	0%	0%	0%	0%
leg (hairy)	100%	0%	0%	0%	0%	0%	0%
meat, $8°C$	5.1%	94.1%	0%	0%	0.8%	0%	0%
meat, $36°C$	0%	100%	0%	0%	0%	0%	0%
meat, $36°C$ [1]	14.8%	28.9%	7.4%	12.9%	26.2%	7.4%	2.4%
meat, $36°C$ [2]	14.7%	8.2%	12.9%	14.1%	28.2%	21.9%	0%
chair coat [3]	0%	0%	71.5%	0%	0.8%	27.7%	0%
plastic box	0%	0%	19.5%	75.4%	0.4%	4.7%	0%
brown carton	0%	0%	4.7%	0%	0%	95.3%	0%
wood block	0%	0%	0%	0%	98.4%	1.6%	0%

[1] with thin ash layer
[2] with thicker ash layer
[3] polyester fabric

The samples used for the experiment are different from the ones the classifier has been trained with. The wood samples were roughly of the same cultivar because different cultivars have different NIR spectra. Different polymers also have different spectra, which is why several subclasses should be trained to distinguish e. g. plastics material from clothes made of polyester.

An extra series of measurements have been taken with meat of different temperatures and layered with different thicknesses of coal ash. The set-up of this series is shown in Fig. 8. Fig. 9 shows the averaged spectra of meat and skin in comparison.

It strikes out, that the spectra of skin and meat are very distinctive in comparison to the other materials and similar among each other. No sample other than skin or meat was classified as one of the two, i. e. no false positives occured

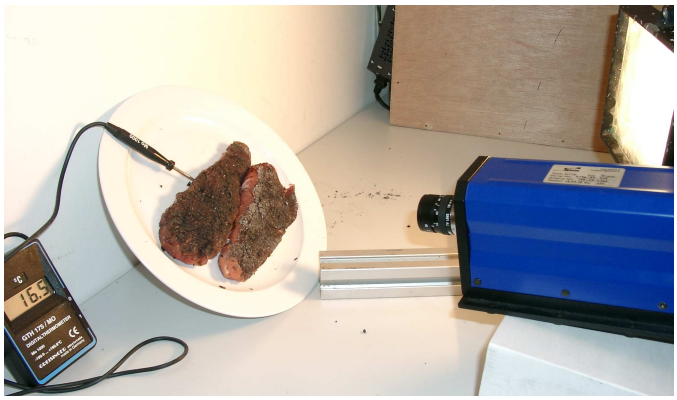

Fig. 8. Experimental set-up, here: pork with a layer of coal ash.

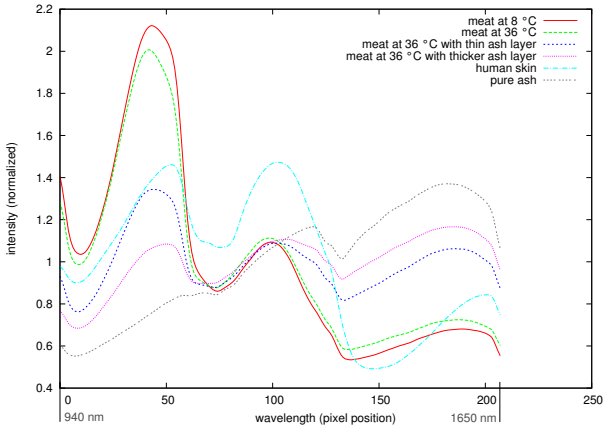

Fig. 9. NIR spectra of meat at different temperatures and ash layers and spectra of skin in comparison.

in the two classes. With a thin ash layer meat was detected 28.9%, with a thicker layer still 8.2%. With a growing thickness the spectra adapt to those of pure ash (see Fig. 9). Thus it seems, that in the presence of little ash a certain rate of radiation is still reflected by the meat underneath and with a growing thickness it shrinks until the rate of radiation reflected by pure ash is at 100%.

The results evolving from a stricter rejection threshold of 5° show, that the organic substances pure meat and leg (hairy) are still detected at a rate of over 62%. This indicates a very high differentiation rate of the spectra of those substances. Meat with a thin ash layer is in this case detected 5%.

V. Future Work

In this paper we concentrated on the enhancement of hyperspectral images and on the classification of single spectra with a very simple classifier, also with low training effort. In addition we considered only a small subset of materials which are present in a real USAR environment.

The classification of the materials could easily be enhanced for critical materials by using more than one model spectrum for one material class. For example the classification of skin with the presence of ash could be enhanced by introducing skin subclasses, with different grades of ash present. A more sophisticated classification approach or the usage of mixture models may also enhance the classification results.

Another approach to enhance the results is to make use of the spatial information in the image. By applying basic image processing techniques like filter operations, the results could be enhanced by combining the classification results in a neighborhood. For a stable victim detection also higher level image processing algorithms like segmentation and shape recognition are required and will certainly enhance the overall classification. However these techniques cannot be applied to images with just one spatial dimension. The second spatial dimension could be realized by a rotating or tilting mirror.

VI. Conclusion

We have shown that hyperspectral imaging in the bandwidth of NIR is a promising technique for victim detection. It has the advantage that different materials can be distinguished and that even small patches of human matter such as skin or clothes suffice for a reliable detection. Even bodies covered with a thin ash layer, a condition in which color image analysis fails, and undercooled bodies, which cannot be detected by thermal imaging, can be detected with this technique. It is very likely that further improvements, as described in Sect. V, lead to even better classification results. The only drawbacks are the dimension and the weight of hyperspectral cameras and the necessity of a strong radiation source.

References

[1] Til Aach and Volker Metzler. Defect interpolation in digital radiography - how object-oriented transform coding helps. In M. Sonka and K. M. Hanson, editors, *SPIE Vol. 4322: Medical Imaging 2001*, pages 824–835, San Diego, USA, February 17–22 2001. SPIE.

[2] Dirk Balthasar, Thomas Erdmann, Johannes Pellenz, Volker Rehrmann, Jörg Zeppen, and Lutz Priese. Real-time detection of arbitrary objects in alternating industrial environments. *In Proceedings Scandinavian Conference on Image Analysis*, 1:321–328, 6 2001.

[3] James E. Burger. *Hyperspectral NIR Image Analysis. Data Exploration, Correction and Regression.* PhD thesis, 2006.

[4] Helmut Günzler and Harald Böck. *IR-Spektroskopie*. VCH, 1983.

[5] Manfred Hesse, Herbert Meier, and Bernd Zeeh, editors. *Spektroskopische Methoden in der organischen Chemie*. Georg Thieme Verlag, 5 edition, 1995.

[6] A. Kulcke, C. Gurschler, G. Spöxk, R. Leitner, and M.Kraft. On-line classification of synthetic polymers using near infrared spectral imaging. In *NIR Publications 2003*, pages 71–81, 2003.

[7] Robin Murphy, Satoshi Tadokoro, Daniele Nardi, Adam Jacoff, Paolo Fiorini, Howie Choset, and Aydan Erkmen. Search and rescue robotics. In Bruno Siciliano and Oussama Khatib, editors, *Springer Handbook of Robotics*, chapter 50, pages 1151–1174. Springer, 2008.

[8] W. Press, W. Vetterling, S. Teukolsky, and B. P. Flannery. *Numerical Recipes in C++: the art of scientific computing*. Camebridge University Press, 2002.

[9] A. Savitzky. Smoothing and differentiation of data by simplified least squares procedures. *Analytical Chemistry*, 36:1627–1639, 1964.

[10] Werner Schmidt. *Optische Spektroskopie. Eine Einführung*. Wiley-VCH, 2 edition, 2000.

[11] Daniel P. Stormont. An online bayesian classifier for object identification. In *Proceedings of the 2007 IEEE International Workshop on Safety, Security and Rescue Robotics*, Logan, USA, 2007. IEEE.

[12] Victor R Weidner and Jack J. Hsia. Reflection properties of pressed polytetrafluoroethylene powder. *Journal of the Optical Society of America*, 71:856–861, 1981.

[13] Roberta Yuhas, Alexander Goetz, and Joe Boardman. Discrimination among semi-arid landscape endmembers using the spectral angle mapper (sam) algorithm. In *Summaries of the Third Annual JPL Airborne Geoscience Workshop*, volume 1, pages 147–149, 1992.